Curvature Driven Flow of Thin Polymer Films and Diffusivity Measurements

Ioannis Karapanagiotis*,† and William W. Gerberich‡

"Ormylia" Art Diagnosis Center, Ormylia, Chalkidiki 63071, Greece, and Department of Chemical Engineering and Materials Science, University of Minnesota, Minneapolis, Minnesota 55455

Received September 1, 2004; Revised Manuscript Received January 21, 2005

ABSTRACT: We study the leveling process of nanoindentation-induced defects on polystyrene (PS) films (h = 100−150 nm) spin cast on silicon (Si) surfaces. Leveling occurs upon annealing above the glass transition temperature (T_g) of bulk PS, resulting in a flat polymer surface. The dynamics of the process is recorded with an AFM for PS molecular weights lower and comparable to the critical entanglement point. Diffusivity values measured from the recorded curvature driven flow are found to be in a very good agreement with corresponding self-diffusivity values of bulk PS.

1. Introduction

Wetting and dewetting of polymer coatings, thinner than a sessile drop flattened by gravity,[1] have become major research topics,[2−5] as polymer films find extensive applications in microelectronics, cultural heritage protection, and printing technology and are also used as membranes, adhesives, and paints. Within this framework, numerous investigations have been performed to study the stability of these films,[6,7] whenever applied onto a hard nonwettable surface.[8−12] For experimental studies, polystyrene (PS) film on silicon (Si) surface has been extensively utilized as a typical-model bilayer system for analogous investigations.[10−18] It has been found that for films with film thickness (h) less than 100 nm dewetting occurs, upon heating above the glass transition temperature (T_g) of the polymer. In thicker films dewetting can be initiated only by, external, surface or interfacial defects.[8,9,16,19] The (de)wetting dynamic evolution of thin films upon heating above T_g has been exploited to measure and investigate thin film properties such as density,[20] viscosity,[21,22] contact angle with the substrate,[23,24] surface energy,[25] and surface glass transition temperature.[26] Following this spirit we have measured surface diffusivity values of low molecular weight (M = 10 900 g/mol) PS by recording the leveling process of an indent induced by a probe on a PS film on Si as a function of temperature and found to be in relatively good agreement with the self-diffusivity of PS.[27] In the present investigation, we examine this finding by keeping the annealing temperature constant (110 °C) and varying the molecular weight of the tested PS samples. Molar masses are shown in Table 1 along with the corresponding calculated radius of gyration (R_g) and surface tension (γ) of PS.[28]

A nanoindentation device, used typically to measure mechanical properties of films, was utilized to induce surface disturbances on PS films (h > 100 nm) on Si at room temperature. The residual depth of penetration (z_D) was lower than the film thickness (z_D < h). For thin (h < 100 nm) films, these kind of defects can either grow toward the substrate and initiate dewetting or can heal level, resulting in a flat surface, upon heating above T_g.[18] In the present study all indents healed. The leveling evolution was monitored using an atomic force microscope (AFM).

Table 1. PS Properties: Radius of Gyration, R_g, and Surface Tension, γ, at 110 °C[28]

M_w (g/mol)	M_w/M_n	R_g (nm)	γ (mN/m)
13 700	1.06	3.3	33.8
18 700	1.07	3.8	33.9
29 300	1.09	4.7	34.0
44 000	1.08	5.8	34.1

In the following we first describe the materials and the experimental setup. We then provide a short description of the topographical changes that occur during an indent healing process. Considerations associated with the interactions that might contribute to this leveling process are then discussed. Curvature measurements in the thin regions (indents) are presented followed by diffusivity measurements. Finally, the effects (i) of the nanoindentation induced residual stresses and (ii) of the shear strain rate on the diffusivity measurements are evaluated.

2. Experimental Section

Monodisperse PS with various molecular weights (Aldrich Chemical Co., Milwaukee, WI) shown in Table 1, was dissolved in spectroscopic grade toluene. Solutions of 5 wt % were applied onto 50 mm diameter silicon wafers (Virginia Semiconductor, Fredericksburg, VA) by spin-coating in a clean room of class 100. Samples were then dried in a vacuum chamber at 90 °C < T_g (=93 °C for M_w = 13 700 g/mol) overnight. Ellipsometry was used to measure the thicknesses of the resulting films and found to be in the range 100−150 nm, depending on the molecular weight and spinning rate. The ⟨100⟩ oriented Si wafers were used as they were received by the supplier and contained a 1.7 nm thick native oxide layer. The resulting polymer films are expected to be unentangled (for PS M_c = 38 000 g/mol), except for the samples produced by the 44 000 g/mol PS, which however does not differ substantially from the critical entanglement point.[29]

Nanoindents, with penetration depths lower than the film thicknesses, were imposed on the samples using a nanoindentation Hysitron Triboscope (Hysitron Inc., Minneapolis, MN) mounted with a standard three-sided pyramid (Berkovich)

† "Ormylia" Art Diagnosis Center.
‡ University of Minnesota.
* Corresponding author: e-mail g.karapanagiotis@artdiagnosis.gr; Tel 011 30 23710 98400; Fax 011 30 23710 98402.

10.1021/ma048216z CCC: $30.25
Published on Web 03/05/2005

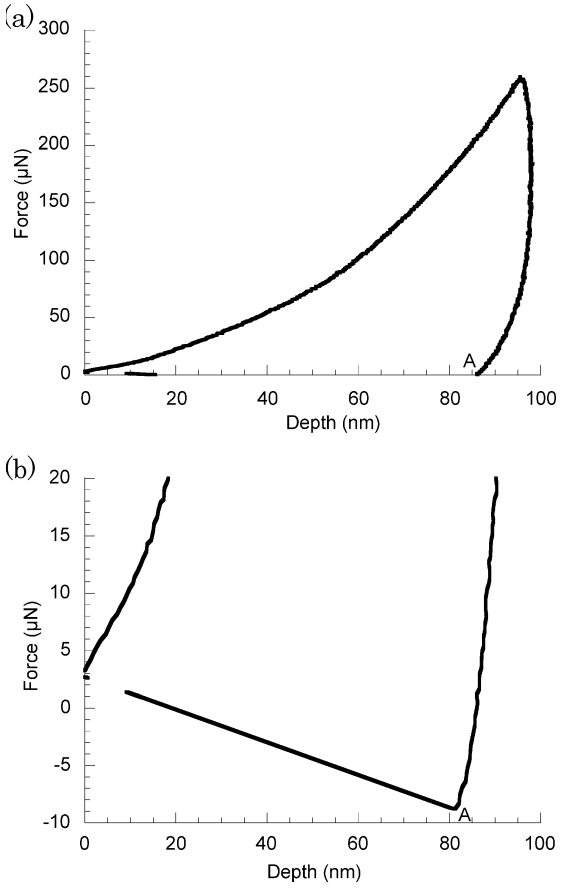

Figure 1. (a) Force−displacement curve of nanoindentation and (b) corresponding enlargement at point A showing the negative adhesive force developed between the indenter probe and a PS film.

diamond tip of nominal radius of curvature 300 nm. The nanoindentation device adapts to an AFM which utilizes a Hysitron microsensor system instead of the standard AFM head component for applying loads electrostatically. The Hysitron Triboscope is a load controlled instrument. The loads required to induce shallow indents, with depths of penetration lower than the film thicknesses, were determined by preliminary experiments at which a series of nanoindentations were induced under different loads and imaged by AFM to measure the residual depths. The load range, finally used, was determined to be 230−270 μN. Deep indents, visible with an optical microscope, imposed under high forces (11 mN) served as markers to locate the indentation area and position the AFM tip at the vicinity of the shallow indents. Imaging was performed using a Nanoscope III SPM (Digital Instruments, Santa Barbara, CA) operated in the contact mode and mounted with a standard silicon nitride probe. Forces in the range of 1−10 nN were applied from the 200 μm cantilever to the polymer surface. Repeated scanning of the same surface area showed no alteration of the recorded topography due to the applied scanning force.

The dynamics of the healing−leveling process of the imposed indents upon heating at 110 °C > T_g was recorded by AFM, following a cyclic procedure of heating at 110 °C and then quenching at room temperature and imaging. The evolution of each indent was monitored, for several anneal−quench cycles, before resulting in a flat surface identical to the rest of the free polymer surface. For all image acquisitions the same AFM probe was used.

3. Results and Discussion

Leveling Process. Figure 1a shows a typical force−displacement (depth of penetration) curve obtained by a Hysitron triboscope, and Figure 1b is a magnification of the vicinity of point A at which the indenter tip withdraws from the sample. A negative force, shown in Figure 1b, corresponds to an adhesive, "pull-off" force between the diamond tip and the film. The presence of such force is indicative for soft, polymeric samples and suggests that the accurate measurement of the residual depth of penetration cannot be performed using load−displacement curves but requires imaging of the residual indent. Indentations, such as the one shown in Figure 1, resulted in indents with triangular top view shapes because of the three-sided pyramid (Berkovich) tip which was used for the nanoindentation tests.[27] Upon heating above T_g, an indent evolves to circular. This (leveling) process is shown in Figure 2. The vertices and the sides of the initial triangle become round as the indent "expands" laterally, resulting gradually in a flat

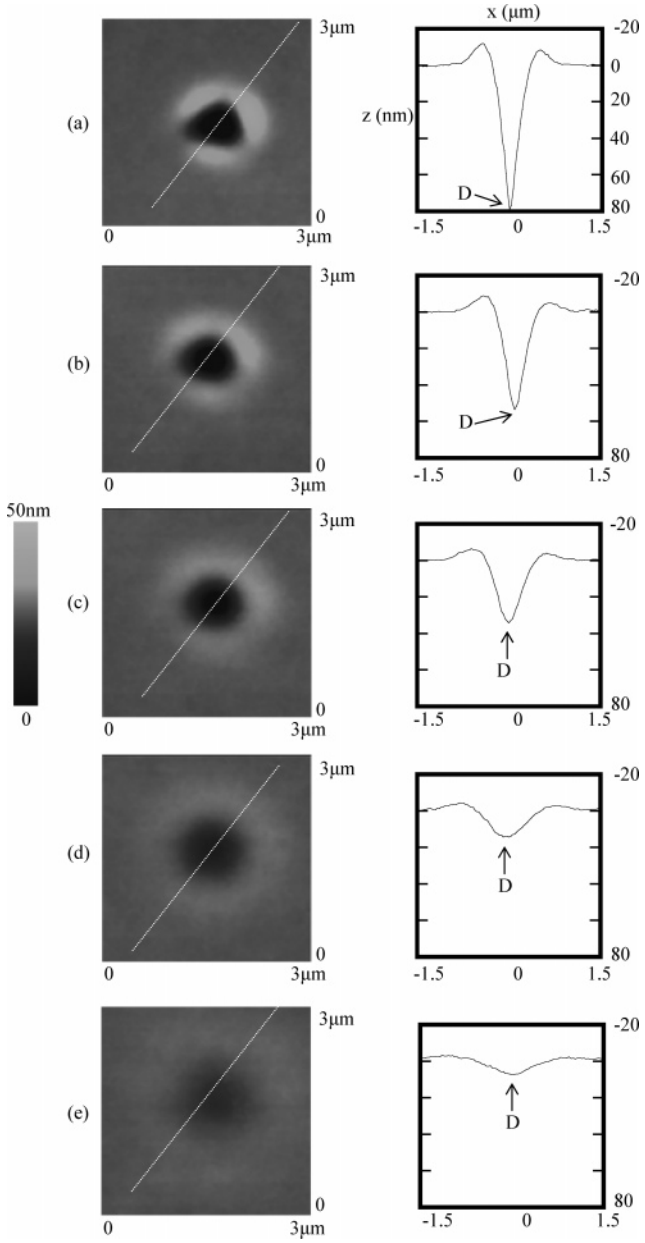

Figure 2. AFM images and corresponding cross sections showing the leveling process of a nanoindent, induced by a Berkovich tip, upon annealing for (a) 2.13, (b) 6.38, (c) 11.13, (d) 21, and (e) 33.25 min, at 110 °C. Point D corresponds to the maximum indent depth, defined as z_D. The molecular weight of the PS film was M_w = 18 700 g/mol.

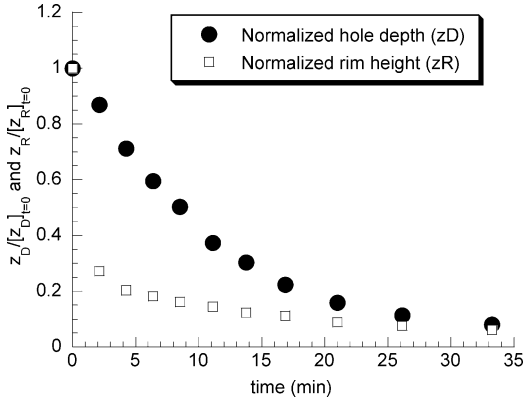

Figure 3. Indent depth, z_D, and maximum rim height, z_R, normalized to their respective values at $t = 0$ as a function of annealing time for PS with $M_w = 18\,700$ g/mol.

surface, similar to the rest of the free polymer surface.[30] This evolution is accompanied by an increase of the surrounding rim width and indent diameter and an apparent decrease of the rim height and indent depth.[27]

Interactions Affecting the Leveling Process. From all the topographical changes occur during the healing−leveling process, described above, we focus in this study in the upward motion of the indent bottom, defined as point D in Figure 2. This motion is driven and can be affected by the following: (i) the mean curvature of the hole at the vicinity of point D, (ii) the relaxation of the surrounding rim, (iii) the van der Waals (VDW) interaction developed between the film and the substrate, (iv) the geometrical restrictions imposed by the small film thickness, and (v) the residual stress field induced by nanoindentation. Finally, one should evaluate also possible effects of shear rate on the leveling process, considering that the latter is recorded at a low temperature (110 °C) which is close to the T_g of bulk PS. The mean curvature effect is essentially the topic of this article and will be investigated in detail later. We will describe the dynamics of the hole healing process as a curvature driven flow. For a number of reasons that are provided below, the initial stages of the leveling process were not taken into account. In particular, diffusivity measurements were based on AFM images obtained after annealing the samples at 110 °C for more than ∼190 s. Images at the early annealing stages (annealing time <190 s) were not used to interpret the leveling process of the induced nanoindents. The rim relaxation process is faster than the hole healing process;[30] i.e., the relaxation of a surface perturbation is faster in thick than in thin regions.[31,32] This is shown in Figure 3 where the indent depth, z_D, normalized to its respective value at $t = 0$, $[z_D]_{t=0}$, and the normalized maximum rim height, $z_R/[z_R]_{t=0}$, are plotted as a function of annealing time. The rim height decreases very fast to a very small value, close to zero, compared to the hole depth. Consequently, any effect of the rim relaxation on the upward motion of the hole bottom should be important at the initial stages of the leveling process. We note here that this abrupt decrease of the rim height at short annealing times might be affected by the lateral shape change (from triangular to circular) of the indent. Thin PS films (<100 nm) spontaneously dewett from Si surfaces because of the dominant unfavorable VDW interactions developed between the two materials. As the films used in this study are relatively thick (>100 nm) spontaneous dewetting does not occur. However, VDW forces developed at the indent bottom might be important (but not dominant as indents level) because of the local thinning of the film. If the latter is true, VDW should be important at the initial stages when the separation distance between the hole bottom and the substrate is minimum.[33] Although chain sizes (Table 1) are substantially lower than film thicknesses (100−150 nm) geometrical restrictions might play a role at the vicinity of the hole bottom where the local film thickness is initially and prior to thermal treatment on the order of 10−30 nm. As an indent heals, however, and the local film thinning is relieved, any effect rising from the restricted thickness should be diminished. The effects of the residual stresses and shear strain rate on the leveling process are evaluated later, after diffusivity measurements.

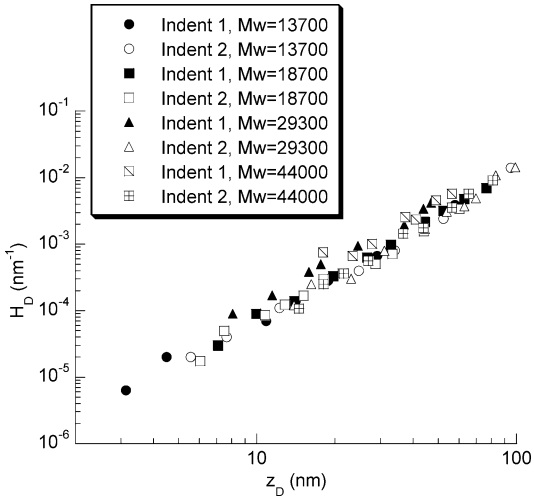

Figure 4. Curvature of indent bottom, H_D, vs indent depth, z_D. Data correspond to eight indents.

Curvature Measurements. The dynamics of eight total indents were recorded for the PS films of Table 1 (two indents for each molecular weight). Indent depths, z_D, were measured directly from AFM cross sections. The latter were also used to calculate mean curvatures, H_D, at the indent bottoms. The results are presented in Figure 4. Curvature calculations were based on the definition of the mean local curvature of a surface at a point D:

$$H_D = \frac{1}{2}\left(\frac{1}{R_1}\bigg|_D + \frac{1}{R_2}\bigg|_D\right) \quad (1)$$

where R_1 is the minimal and R_2 the maximal value of the curvature R of a section normal to the surface at point D. In 2 dimensions, the curvature of a curve $y = f(x)$ at a given point (x_D,y_D) is defined as

$$\frac{1}{R}\bigg|_{(x_D,y_D)} = \frac{|f''(x_D)|}{[1 + f'(x_D)^2]^{3/2}} \quad (2)$$

By fitting the indent bottom cross section with a $f(x)$ fourth-order polynomial function, H_D was calculated using eqs 1 and 2. We note here that H_D is the mean local curvature at point D, and it is higher than the curvature of any other point of the indent. Also, point D is the only indent surface point that performs a motion in one, perpendicular to the substrate, direction during the leveling process. All the other points of the

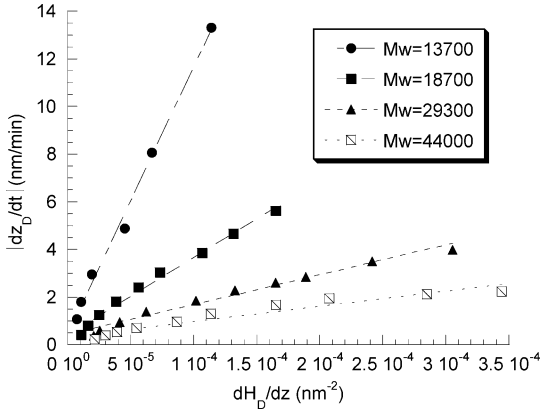

Figure 5. Absolute value of the healing rate $|dz_D/dt|$ vs curvature gradient in the vertical direction at point D, dH_D/dz. Linear fits are shown.

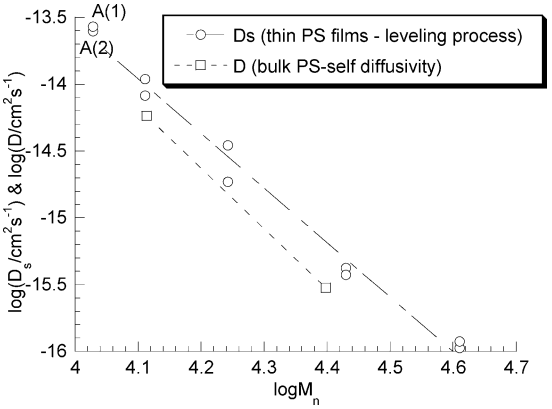

Figure 6. Surface diffusivity, D_s (cm²/s), measured by the leveling process of thin films and self-diffusivity, D (cm²/s), of bulk PS[38,39] vs molecular weight, M_n (g/mol). Points A(1) and A(2) were obtained in another study.[27] Linear fits, with slopes −4 and −4.5 for the thin PS films and the bulk PS, respectively, are shown.

free surface of the indent exhibit along with the perpendicular a lateral motion resulting from the lateral "expansion" of the indent upon leveling (Figure 2).

Diffusivity Measurements. The indent leveling process can be interpreted in terms of a diffusion process. Using the z_D and H_D available data, the healing rate dz_D/dt and the curvature gradient in the vertical direction dH_D/dz, at point D, were calculated. The results for four indents are presented in Figure 5.[36] It can be observed that linear relations can fit the data quite satisfactory. The slopes of these fits can be used to measure diffusivity values according to the following analysis.[27] For isotropic materials, the chemical potential, μ, depends on the curvature by the Gibbs−Thomson relation[37]

$$\mu = \Omega\gamma\left(\frac{1}{R_1} + \frac{1}{R_2}\right) \tag{3}$$

where Ω and γ are the molecular volume and the surface tension, respectively. The molecular volume can be estimated, in our case, as the volume occupied by a coil:

$$\Omega = \frac{4}{3}\pi {R_g}^3 \tag{4}$$

where R_g is the radius of gyration of the PS molecules. The drift velocity along the z-direction, u_z, of surface molecules is given by the Einstein−Nernst relation[37]

$$u_z = -\frac{D_s}{kT}\frac{\partial \mu}{\partial z} \tag{5}$$

where D_s is the surface diffusivity, k the Boltzmann constant, and T the absolute temperature. The velocity is defined as follows:

$$u_z = \frac{dz}{dt} \tag{6}$$

By combining eqs 3−6 and using the definition of H_D given in eq 1, the motion of point D can be described by the following relation:

$$\left|\frac{dz_D}{dt}\right| = \frac{8\pi D_s \gamma {R_g}^3}{3kT}\frac{\partial H_D}{\partial z} \tag{7}$$

Using the slopes calculated from the linear fits of Figure 5, the values of γ and R_g as they are given in Table 1, $k = 1.38 \times 10^{-23}$ J/K and $T = 383.15$ K (=110 °C) diffusivity values were obtained and are presented in Figure 6. In the same plot, PS surface diffusivity values for $M_w = 10\,900$ g/mol ($M_w/M_n = 1.02$), measured similarly to the above analysis, in another study[27] for a 120 nm thick film, are presented and indicated as points A(1) and A(2). For comparison, we also present the self-diffusivity, D, of bulk PS measured by Lodge et al.[38,39] In this case measurements were performed by Forced Rayleigh scattering after labeling PS molecules with a photoisomerizable dye molecule. In both cases, surface film diffusivity and bulk self-diffusivity logarithmic values are presented, and the corresponding linear fits are shown. The slopes of the linear fits are −4 and −4.5 for thin film and bulk PS, respectively.

On the basis of Figure 6, the following observations can be made: (i) A relatively good agreement is obtained between the diffusivities measured by the indent healing process and the self-diffusivity of PS. To establish this conclusion, we further compare our results with the self-diffusion coefficient of bulk PS (1900 g/mol) reported by Ediger et al.[40] At the temperature of interest (110 °C) the self-diffusivity, D, found to be approximately 3.2×10^{-11} cm²/s ($\log D - 10.5$).[40] For illustrative purposes this point is not shown in Figure 6 because it corresponds to a very low molecular weight. From the linear curve fit of our data we calculate that for the same molar mass $D_s = 2.5 \times 10^{-11}$ cm²/s ($\log D_s = -10.6$), which is in excellent agreement with the value of D. Consequently, an indent healing process can be interpreted as a diffusion process, described by a diffusion coefficient close to the self-diffusivity of the polymer. Taking this argument in a reverse way, it can be stated that dynamic properties of thin films can be measured by monitoring the leveling process of a well-characterized surface disturbance. (ii) An augmented deviation from the Rouse model ($D \sim M^{-1}$) has been recorded in our measurements, similar to the data obtained by Lodge. This deviation rises mainly because of the glass transition temperature variation occurring in the investigated molecular weight range. If we adjust T_g variations, a relation closer to the Rouse dynamics can be obtained, as shown below. For the bulk PS data shown in Figure 6 the constants C_1^g and C_2^g of the Williams−Landel−Ferry (WLF) equation have been reported, along with

Table 2. Properties of Bulk PS[38]

M (g/mol)	C_1^g	C_2^g	T_g (°C)	D_g (cm²/s)	R_g[a] (nm)
13 000	12.80	83.22	92.6	3.389×10^{-17}	3.3
25 000	11.67	52.73	99.1	2.957×10^{-18}	4.5

[a] Radii of gyration were calculated as in Table 1.[28]

the corresponding diffusivity D_g values at T_g, according to Table 2.[38] The WLF equation is

$$\log\left(\frac{DT_g}{D_gT}\right) = \frac{C_1^g(T - T_g)}{C_2^g + (T - T_g)} \tag{8}$$

Using eq 8 and the data of Table 2, diffusivity values at $T = T_g + 10$ °C are found to be 8.220×10^{-16} and 2.202×10^{-16} cm²/s for 13 000 and 25 000 g/mol, respectively. If we plot these values with respect to molecular weight, we find that $D \sim M^{-2}$. This result approaches the expected Rouse dynamics, and it is almost identical with the corresponding relation reported for the self-diffusion coefficient of polyethylene.[41] A similar result is apparently obtained if we treat the data for the thin PS films in the same way. Other effects that should be considered as influencing parameters on the recorded dynamics are the molecular weight dependence of the monomeric friction factor, ζ_0, as well as chain-end effects, augmented due to the short length of the chains. In addition to the above, which are known for bulk polymers, the interactions described previously as potential influencing parameters of the healing process of the PS films might also have a minor contribution to the observed deviation from the Rouse model. However, as it has been argued, these interactions should not be dominant after continuous heating above T_g. Attempts to evaluate the effects of the residual stresses and shear rate on the leveling process are discussed next.

Effect of Residual Stresses. Surface disturbances (indents) studied in this investigation were imposed by nanoindentation. Consequently, a stress field around a residual indent should be present. Continuous heating at temperatures above the T_g results in the relaxation of these stresses. At 110 °C, residual stresses induced on the films of low molecular weight PS are lower than the Laplace pressure, developed because of the indent curvature, as it has been discussed in a previous study.[30] However, because indents were induced at room temperature, it is necessary to estimate the characteristic (longest) relaxation time, τ_1, and compare it with the time scale of the recorded leveling process, considering that the data used for diffusivity measurements were obtained after annealing the samples at 110 °C for ~190 s. For short polymer chains ($M < M_c$) the characteristic relaxation time, τ_1, varies as[42]

$$\tau_1 = \frac{M^2 {l_0}^2 \zeta_0}{6kT{M_0}^2\pi^2} \tag{9}$$

where M_0 is the molecular weight of the repeat unit with length l_0. The self-diffusivity is given by

$$D = \frac{kTM_0}{M\zeta_0} \tag{10}$$

The radius of gyration can be expressed in terms of l_0 as follows:

$$R_g = l_0\sqrt{\frac{M}{6M_0}} \tag{11}$$

Using eqs 10 and 11, eq 9 can be rewritten to provide τ_1 as a function of the self-diffusivity and the radius of gyration:

$$\tau_1 = \frac{{R_g}^2}{\pi^2 D} \tag{12}$$

By taking D values for bulk PS as they are shown in Figure 6 ($D = 5.80 \times 10^{-15}$ and 3.04×10^{-16} cm²/s) and R_g values given in Table 2, τ_1 is found to be 1.9 and 67.5 s for 13 000 and 25 000 g/mol, respectively, shorter than the annealing period of 190 s, before which the received data (curvature measurements by AFM) were not used for diffusivity calculations. Using now diffusivities, D_s, determined by the leveling of the films and R_g given in Table 1, the longest relaxation times are calculated to be <60 s for all molecular weights, except for the highest one ($M_w = 44\,000$ g/mol), for which τ_1 is found to be on the order of 300 s = 5 min (>190 s). We note here that in this case the leveling process was completed in ~90 min. Therefore, the majority of the data points were obtained after substantial annealing at 110 °C, upon which mechanical stresses should have been relaxed, except from one (the first) data point obtained after ~190 s of heating. This particular point, however, did not affect the resulting D_s values, as it was verified upon extracting this point from our calculations.

Effect of Shear Strain Rate. In this paragraph we discuss possible shear strain rate effects on the diffusivities measured in this study. Shear rate effects can be evaluated by estimating the following dimensionless parameter, β:[22]

$$\beta = \frac{\eta_0 M_w \dot{\gamma}}{\rho RT} \tag{13}$$

where η_0 and ρ are the zero shear viscosity and the density of the material respectively, $\dot{\gamma}$ is the shear strain rate, and R is the gas constant. If $\beta < 10$, then shear rate effects can be considered as negligible. For unentangled polymers, the zero shear rate viscosity is given by[42]

$$\eta_0 = \frac{\zeta_0 M N_{av} \rho {l_0}^2}{36{M_0}^2} \tag{14}$$

By combining eqs 10, 11, 13, and 14, parameter β can be expressed as a function of diffusivity:

$$\beta = \frac{M_w \dot{\gamma} {R_g}^2}{6DM} \tag{15}$$

In the following we first calculate the parameter β for the high molecular weight PS ($M_w = 44\,000$ g/mol), for which shear rate effects should be pronounced, compared to the smaller PS molecules. For the calculations we consider the lowest diffusivity determined for this molecular size, $D_s = 1.06 \times 10^{-16}$ cm²/s, according to Figure 6, because this will result to the highest value of β. The radius of gyration is taken as $R_g = 5.8$ nm according to Table 1. The shear rate, $\dot{\gamma}$, of the leveling process can be estimated as $\dot{\gamma} = \mathrm{d}(\tan\theta)/\mathrm{d}t$, where θ is the angle defined as $\tan\theta = 2z_D/d$. Here, d is the indent

diameter at the level of the initially unperturbed PS surface ($z = 0$, of Figure 2) and z_D is the indent depth. Having z_D and d from the AFM images as a function of time, the shear rate is found to be on the order of 0.006 s^{-1}, resulting in $\beta = 3.4$. Following the same approach, we calculated that for $M_w = 29\,300$ g/mol β is on the order 2.5, while for lower M_w, $\beta < 1$. In all cases $\beta < 10$, resulting in the conclusion that shear strain rate effects do not have any substantial impact on the leveling process of the nanoindents.

4. Conclusions

The dynamics of the leveling process of surface disturbances, induced by nanoindentation, in thin (100−150 nm) films of low molecular weight PS on Si surfaces was recorded by AFM. Leveling occurs upon annealing above T_g. Diffusivity coefficients, measured at 110 °C, for a molecular weight range of 10 900−44 000 g/mol, were found to be in very good agreement with the corresponding self-diffusivity values of bulk PS. Consequently, the leveling process of a well-characterized surface disturbance can be interpreted as a curvature driven flow and can be used to measure dynamic properties of thin polymer films. Diffusivities were measured after annealing the samples at 110 °C for ∼3 min to allow nanoindentation-induced residual stresses to relax and to suppress the effects of other interactions such as VDW forces between the film and the substrate, surrounding rim relaxation, and geometrical restrictions.

Acknowledgment. Support by the Center for Interfacial Engineering (CIE), a National Science Foundation Engineering Research Center, is gratefully acknowledged. The authors also acknowledge T. P. Lodge for valuable discussions.

References and Notes

(1) Taylor, G. I.; Michael, D. H. *J. Fluid Mech.* **1973**, *58*, 625−639.
(2) de Gennes, P. G. *Rev. Mod. Phys.* **1985**, *57*, 827−863.
(3) Kheshgi, H. S.; Scriven, L. E. *Chem. Eng. Sci.* **1991**, *46*, 519−526.
(4) Müller-Buschbaum, P. *J. Phys: Condens. Matter* **2003**, *15*, 1549−1582.
(5) Geoghegan, M.; Krausch, G. *Prog. Polym. Sci.* **2003**, *28*, 261−302.
(6) Ruckenstein, E.; Jain, R. K. *J. Chem. Soc., Faraday Trans.* **1974**, *70*, 132−147.
(7) Sharma, A.; Ruckenstein, E. *J. Colloid Interface Sci.* **1986**, *113*, 456−479.
(8) Brochard-Wyart, F.; Daillant, J. *Can. J. Phys.* **1990**, *68*, 1084−1088.
(9) Redon, C.; Brochard-Wyart, F.; Rondelez, F. *Phys. Rev. Lett.* **1991**, *66*, 715−718.
(10) Sharma, A.; Reiter, G. *J. Colloid Interface Sci.* **1996**, *178*, 383−399.
(11) Müller-Buschbaum, P.; Stamm, M. *Physica B* **1998**, *248*, 229−237.
(12) Müller, M.; MacDowell, L. G.; Müller-Buschbaum, P.; Wunnike, O.; Stamm, M. *J. Chem. Phys.* **2001**, *115*, 9960−9969.
(13) Reiter, G. *Phys. Rev. Lett.* **1992**, *68*, 75−78.
(14) Reiter, G. *Langmuir* **1993**, *9*, 1344−1351.
(15) Müller-Buschbaum, P.; Vanhoorne, P.; Scheumann, V.; Stamm, M. *Europhys. Lett.* **1997**, *40*, 655−660.
(16) Stange, T. G.; Hendrickson, W. A.; Evans, D. F. *Langmuir* **1997**, *13*, 4459−4465.
(17) Xie, R.; Karim, A.; Douglas, J. F.; Han, C. C.; Weiss, R. A. *Phys. Rev. Lett.* **1998**, *81*, 1251−1254.
(18) Karapanagiotis, I.; Evans, D. F.; Gerberich, W. W. *Langmuir* **2001**, *17*, 3266−3272.
(19) Karapanagiotis, I.; Gerberich, W. W.; Evans, D. F. *Langmuir* **2001**, *17*, 2375−2379.
(20) Reiter, G. *Macromolecules* **1994**, *27*, 3046−3052.
(21) Cole, D. H.; Shull, K. R.; Baldo, P.; Rehn, L. *Macromolecules* **1999**, *32*, 771−779.
(22) Masson, J. L.; Green, P. F. *Phys. Rev. E* **2002**, *65*, 031806/1−031806/5.
(23) Reiter, G.; Khanna, R. *Phys. Rev. Lett.* **2000**, *85*, 2753−2756.
(24) Reiter, G.; Khanna, R. *Langmuir* **2000**, *16*, 6351−6357.
(25) Choi, S. H.; Newby, B. Z. *Langmuir* **2003**, *19*, 1419−1428.
(26) Erichsen, J.; Kanzow, J.; Schürmann, U.; Dolgner, K.; Günther-Schade, K.; Strunskus, T.; Zaporojtchenko, V.; Faupel, F. *Macromolecules* **2004**, *37*, 1831−1838.
(27) Karapanagiotis, I.; Evans, D. F.; Gerberich, W. W. *Polymer* **2002**, *43*, 1343−1348.
(28) Brandrup, J.; Immergut, E. H. *Polymer Handbook*, 3rd ed.; John Wiley: New York, 1989.
(29) Fox, T. G.; Gratch, S.; Loshaek, S. In *Rheology*; Eirich, F. R., Ed.; Academic Press: New York, 1956; Vol. 1, Chapter 12.
(30) Karapanagiotis, I.; Evans, D. F.; Gerberich, W. W. *Macromolecules* **2001**, *34*, 3741−3747.
(31) Kheshgi, H. S. Ph.D. Thesis, University of Minnesota, 1983.
(32) Keunings, R.; Bousfield, D. W. *J. Non-Newtonian Fluid Mech.* **1987**, *22*, 219−233.
(33) VDW interaction force F_{VDW} between two bodies scales with the separation distance z according to[34,35] $F_{VDW} \sim z^{-3}$ for two planar surfaces and $F_{VDW} \sim z^{-2}$ for a sphere and a planar surface. The latter might be applied as an approximation, in our case, if we simulate the indent bottom with a sphere of radius $1/H_D$, where H_D is the curvature at the indent bottom (point D).
(34) Evans, D. F.; Wennerstrõm, A. *The Colloidal Domain*; VCH Publishers: New York, 1994.
(35) Israelachvili, J. N. *Intermolecular & Surface Forces*; Academic Press: San Diego, CA, 1991.
(36) Because indent depth values were taken as positive numbers (Figure 2), the healing rate dz_D/dt is a negative number. To eliminate the negative sign, the absolute value $|dz_D/dt|$ is plotted in Figure 5.
(37) Mullins, W. W. *J. Appl. Phys.* **1957**, *28*, 333−339.
(38) Eastman, C. E. Ph.D. Thesis, University of Minnesota, 1993.
(39) Eastman, C. E.; Lodge, T. P. *Macromolecules* **1994**, *27*, 5591−5598.
(40) Urakawa, O.; Swallen, S. F.; Ediger, M. D.; von Meerwall, E. D *Macromolecules* **2004**, *37*, 1558−1564.
(41) Pearson, D. S.; Ver Strate, G.; von Meerwall, E.; Schilling, F. C. *Macromolecules* **1987**, *20*, 1133−1141.
(42) Hiemenz, P. C. *Polymer Chemistry*; Marcel Dekker: New York, 1984.

MA048216Z